INSTITUTE OF PLASMA PHYSICS

NAGOYA UNIVERSITY

RESEARCH REPORT

NAGOYA, JAPAN

SPECTROSCOPIC OBSERVATION OF A QUASI-STEADY STATE OF A PLASMA ON CONTACT WITH A NEUTRAL GAS

Masamoto Otsuka, Ryuiti Ikee*
and
Kazushige Ishii

IPPJ-189 February 1974

Further communication about this report is to be sent to the Research Information Center, Institute of Plasma Physics, Nagoya University, Nagoya, Japan.

---

*Permanent Address: Faculty of Science, Hiroshima University.

This work was carried out under the Collaborating Research Program at Institute of Plasma Physics, Nagoya University, Nagoya, Japan.

Abstract

When a neutral gas (He) is introduced into the "plasma region" of the TPD machine, an intense glow was observed at the tail of a plasma column. The population densities of the excited levels of helium ion He^+ in the glow plasma were found to be much larger than those values expected in a steady state which had the same values of electron temperature and density as observed one; it is shown that the palsma should be considered to be in a quasi-steady state.

I. INTRODUCTION

The "glow plasma" which is observed in the TPD machine as a contact phenomena of a helium plasma with a neutral helium gas has favorable features for spectroscopic investigation of the plasma.

Recombination continua with large intensities are emitted over the glow plasma region, which enable one to determine the electron temperature without ambiguity. Preliminary measurements have already shown that partial local thermodynamic equilibrium prevails among the excited levels of the neutral helium atoms; excitation temperatures have been found to be in a fairly good agreement with the electron temperatures. On the contrary under the normal operation of TPD the intensities of continuum spectra are too small to be measured accurately, and those of line spectra decrease so rapidly towards the series limits that exact excitation temperatures cannot be obtained and yet apparent "excitation temperatures" is far lower than those to be expected. The glow plasma is, therefore, supposed to present a base from which the spectroscopic observation can be advanced for further investigation of the mechanism of plasma production in TPD.

In the present article are shown distributions along the plasma column of the electron temperature and the electron density under the glow plasma conditions and some discussions on the plasma states in connection with the population densities of singly ionized helium ions.

II. THE TPD MACHINE

With the TPD machine (Fig.1) the plasma is produced in the following way. Helium gas is introduced on the right hand side into the machine and pumped out with the vacuum pump at the left end and, if necessary, together with the side pump. Discharge runs between the anode and the cathode which is located at a center of a cusped magnetic field, and the plasma produced here is diffused out into the "plasma region" through a hole (8 mm in diameter) of the anode. The normal operation is performed under the following conditions:

gas pressure:	$\sim$4 to 10 torr in the "dishcarge region".
	$\sim 10^{-3}$ torr in the "plasma region".
gas flow:	$\sim$1 torr lit$\cdot$sec^{-1}
discharge current:	$\sim$1 to 100 A
discharge voltage:	$\sim$130 to 200 V
magnetic field:	several kG

At a discharge current of 100 A the electron density is found to be 10^{14} to 10^{15} cm^{-3}, which has already been confirmed by the measurement with 2 mm microwave, HCN laser[10] and CO_2 laser.[11,12]

III. QUALITATIVE DESCRIPTION OF THE CONTACT PHENOMENA

The plasma under the conditions above looks yellow from end to end through the plasma column. In this state another gas flow (He) is additionally introduced into the

"plasma region". With increasing gas pressure the following phenomena are observed. The downstream end of the plasma column (the tail) begins to glow intensely white and the glowing region shifts toward the anode (to the right). The spectral intensity of the light radiated from a fixed position on the plasma column at first decreases slightly, then increases, reaches maximum at a certain values of pressure and decreases monotonically. The intensity maxima for ion lines appear at pressures lower than those for neutral lines and the widths of the profiles of an intensity vs. pressure curve for the ion lines are narrower than those for neutral lines; the region of the plasma column where ion lines show large intensity is nearer to the anode and smaller than the corresponding region for neutral lines intensities. From these regions are observed radiative recombination continua with large intensity and succeeding line spectra with quantum number up to 17. It is able to fix the glowing region at an arbitrary position by adjusting a leak value with a good reproducibility. The glowing region can be shifted also with other procedures; e.g. downstream with the followings: (1) Decreasing gas flow into the "discharge region". (2) Opening the valve of the side pump. (3) Increasing the discharge current. (4) Decreasing the ratio of the magnetic field intensities B_1/B_2. Since all these procedures prevent the electron temperature from decreasing, it can be considered that with decreasing electron temperature from up to down the plasma stream the doubly ionized ions He^{++} at first begin to recombine with

electrons into singly ionized ones He^+, which in turn become to neutral atoms.

IV. EXPERIEMNTAL

Spectral intensities were observed through five windows with a quartz plate as shown in Fig.1. Windows 2 to 5 are 4 cm wide and 8 cm high. To the part of the inside wall of the vacuum vessel seen through each window (except window 1) is attached a plate preventing light from being reflected, which is composed of 250 sheets of razor-shaped non-magnetic stainless steel plate 0.3 mm thick piled up with the blades to form a surface. A double monochromator (SPEX 1400) was used in order to avoid the error in intensity due to the stray light when calibration is done with a standard lamp; the focal length is 75 cm and the gratings has ruled area of 102 × 102 mm^2 and 1200 grooves per mm blazed at a wavelength of 3000 Å. The entrance, intermediate and exit slit were 200, 400 and 200 μm wide, respectively and the slit height of the entrance slit was 5 mm. The image of the horizontal plasma column was focused on the slit surface through a quartz-fluorite achromatic lens and an image rotator (composed of 3 mirrors) so that it lies parallel to the slit. The magnification was a seventh and the plasma along the column about 3.5 cm long was observed at a time. Spectral intensity was measured at an interval of 0.2 mm across the plasma column and recorded on a punch tape as the total optical system is shifted vertically with a hydraulic press. The observed

intensity distribution has so a good symmetry referred the column axis that the Abel transform[1] to obtain the emission coefficient was performed* with the lower half values for the column (Figs.2 and 3). Detection of light intensity was done by photon counting method with a photo-chopper at a chopping frequency of 150 Hz (SSR, Model 1110, Digital Synchronous Computer). Spectral intensity was calibrated in an absolute scale against a standard lamp with a tungsten ribbon strip.

With a discharge current of 100 A and a fixed configuration of magnetic field and at a rate of gas flow into the "discharge region" of 80 cm^3 min^{-1} (at 20°C and 1 atm.), the leak valve by window 1 was so adjusted that the spectral intensity of HeII 4686 Å observed through window 4 (except for the case specially mentioned) showed a maximum value. Under these conditions the discharge voltage was -130 V at the cathode (with the anode grounded) and the gas pressure were 7.8, 7.3×10^{-3}, 6.0×10^{-3} and 8.0×10^{-4} torr at the cathode, window 2, window 5 and the top of the pump at the left end, respectively.

V. RESULTS

Since the continuum spectrum followed by the triplet diffuse series $n^3D \rightarrow 2^3P$ had the largest intensity among the recombination continua and the curve of the logarithm of intensity vs. wavelength recorded on a chart of a pen-recorder showed a straight line of a constant slope over

* HITAC 8500 was used for the computation.

a wide range of wavelength, the intensity measurement was made at five wave-lengths within this continuum: 2790 Å, 2924 Å, 3052 Å, 3251 Å and 3420 Å. In this range are included the other contimua except that followed by the triplet principal series $n^3P \rightarrow 2^3S$, but they were neglected on the ground that the intensity of the selected contimuum was estimated to be larger than the others at least by one order of magnitude at electron temperatures up to 10 eV and the intensity gap which should appear at the series limit was not observed.

The emission coefficient for the recombination contimuum $\varepsilon(\lambda)$ is given by

$$\varepsilon(\lambda) = \frac{h^7}{8\pi^{9/2} m^3 e^6} \frac{c^2}{\lambda^5} \frac{g}{g^+} \sigma n_e n^+ \left(\frac{E_H}{kT_e}\right)^{\frac{3}{2}} \exp\left[\frac{1}{kT_e}\left(\chi - \frac{ch}{\lambda}\right)\right], \quad (1)$$

where χ is the ionization energy from the excited level of helium 2^3P (= 3.626 eV), E_H the ionization energy of hydrogen (= 13.6 eV), g and g^+ the statistical weights for the levels of HeI 2^3P (= 9) and the ground level of HeII (= 2), n_e and n^+ the particle densities of electrons and singly ionized ions, T_e the electron temperature and the other notations have the usual meanings. For the photo-ionization cross-section σ from the level of HeI 2^3P the following formula[2] was used,

$$\sigma = 10^{26.57} \nu^{-2.9} \qquad (cm^2), \quad (2)$$

where $\nu = c/\lambda$ (sec^{-1}).

Electron temperature was obtained from the tangent of the straight line which shows the relation of $\log(\lambda^5 \varepsilon(\lambda)/\sigma)$ vs. $1/\lambda$, and $n_e n^+$ was calculated from T_e and the absolute value of $\varepsilon(\lambda)$. In the folloiwng the electron density, when assumed $n_e = n^+$, is denoted n_e^*, i.e.,

$$n_e^* = (n_e n^+)^{\frac{1}{2}} \quad , \qquad (3)$$

Figures 4 and 5 show the results as examples.

In Fig.6 T_e and n_e on the axis of the plasma column are shown as a function of the distance from the anode.

In Fig.7 are shown the population densities of levels He^+ (n = 4), He 3^3D and He 4^1D on the column axis which were obtained from the absolute intensities of the lines HeII 4686 Å, HeI 5876 Å and HeI 4922 Å, respectively.

Figure 8 shows the population densities of the levels with the principal quantum number n of 4 to 11 divided by the statistical weights in relation to the excitation energies.

VI. DISCUSSION

At first let the plasma be in a steady state and the measured values be compared with the theoretical ones, for example those by Drawin.[3]

The population densities n_i of level i of He^+ are given by the simultaneous equations

$$\frac{dn_i}{dt} = \sum_j a_{ij} n_j + n_e n^{++} (\alpha_i + n_e Q_i) \quad , \qquad (4)$$

where α_i is the radiative recombination coefficient to level i of He^+, Q_i the three-body recombination coefficient, n^{++} the particle density of He^{++} and a_{ij} the rate coefficient of populating and depopulating processes (see later). In a steady state ($dn_i/dt = 0$) the solutions n_i/n^{++} are obtained with n_e and T_e as parameters. Numerical values of the ratio

$$b_i \equiv (n_i/n^{++})/(n_i/n^{++})_{SAHA} = n_i/(n_i)_{SAHA}$$

are tabulated for two types of excitation cross-sections of He^+: The thereshold value is zero for one and finite for the other. Here $(\ )_{SAHA}$ denotes the value which satisfies the Saha equation with the same n_e, T_e and $n_e{}^{++}$ as in eq.(4).

Under the conditions of the plasma neutrality

$$n_e = n^+ + 2n^{++} \qquad (6)$$

n_i can be fixed as a function of T_e and n_e. Calculation in this manner shows that n_e as a function of T_e has a maximum at $T_e \simeq 10$ eV over the range of 10^{10} to 10^{16} cm^{-3} of n_e as a parameter; n_4 is only 1.9×10^{-3} cm^{-3} even at $T = 2 \times 10^4$ °K, which is higher than the temperature at

window 4, while the measured value of n_e is about 10^{14} cm^{-3}. It is found, therefore, that the present plasma is not in a steady state.

In the next place, estimation is done of the densities n_e, n^+ and n^{++} from eq.(4) with i = 4, in which the measured values of T_e, n_e^* and n_i are substituted. Since the relaxation time of population density of the level is short except that for the ground level[9], it can be assumed for level 4 that $dn_4/dt = 0$; n_4 is given by

$$n_4 = \frac{A' + n_e C' + n_e F' + n_e n^{++} \alpha_4 + n_e^2 n^{++} Q_4}{A + n_e C + n_e F + n_e S_4} , \quad (7)$$

where A, C, F, A', C' and F' are defined as follows:

$$A \equiv \sum_{i<4} A_{4i} , \quad C \equiv \sum_{i>4}^{10} C_{4i} , \quad F \equiv \sum_{i<4} F_{4i} ,$$

$$A' \equiv \sum_{i>4}^{10} n_i A_{i4} , \quad C' \equiv \sum_{i<4} n_i C_{i4} , \quad F' \equiv \sum_{i>4}^{10} n_i F_{i4} ,$$

and A_{jk} is the probability for the spontaneous transition $j \to k$, C_{kj} the rate coefficient for electronic excitation for $k \to j$, F_{jk} the rate coefficient for electronic deexcitation $j \to k$ and S_4 the rate coefficient for ionization from level 4. For the cross-section σ_{kj} for electronic excitation $k \to j$, three different formulas are tried. They are given in the form

$$\sigma_{kj} = 4\pi a_0^2 \left(\frac{E_H}{E_{jk}}\right)^2 f_{kj}\, g(u_{jk}) \quad (8)$$

with

(i)[3,4] $$g(x) = \frac{x-1}{x^2} \ln(1.25x) \quad ,$$

(ii)[3,4] $$g(x) = \begin{cases} 0.302 & 1 \le x \le 3.85 \\ \frac{x-1}{x^2} \ln(1.25x) & x \ge 3.85 \end{cases} \quad ,$$

and

(iii)[5] $$g(x) = \frac{1}{x} \quad ,$$

where a_o is the Bohr radius, E_{jk} the excitation energy $k \to j$, f_{kj} the oscillator strength for absorption $k \to j$, $j_{jk} \equiv E/E_{jk}$ and E the kinetic energy of an electron. The cross-section in case (iii) is given as an approximation by Griem. For the cross-section for electronic ionization is used the formula given by Drawin,[3,4] for α_4 the well-known formula with G-factor assumed to be 1, for A_{jk} and f_{kj} the values given in the Table of NBS.[6] The results are shown in Table 1. Here C_{kj}'s and F_{jk}'s corresponding to the three cases are denoted without superscript, with * and † in case (i), (ii) and (iii), respectively. For lack of measured values some n_i's are assumed, which are shown in parentheses. These assumed values contribute to F' and C', but the contribution to F' are negligible and $n_e C'$ is smaller than the dominant term $n_e F'$ in the numerator of eq.(7) by one, two and four orders of magnitude at window 3, 4 and 5, respectively. Since there are no measured values of n_i for $i > 11$ and their contributions to A', C' and F' would decrease rapidly,

the levels up to 10 are taken into account.

The number densities n_e, n^+ and n^{++} which are obtained as solutions of eqs.(7), (6) and (3) are shown in Table 2 for the three cases of excitation cross-section. From eq. (7) with these values it is found that the dominant term in the denominator is A and that in the numerator is $n_e F'$ (otherwise $n_e n^{++} \alpha_4$ only in case (i) at window 5); level 4 is populated mainly by the cascading process through the upper levels, especially from level 5 and depopulated by spontaneous transition into the lower levels. The difference due to the forms of cross-section is negligibly small at windows 3 and 5, while at window 4 slight difference can be noticed (in case (iii) n^{++} becomes negative!). This seems to be caused by the differences of threshold values of the cross-sections. According to Drawin, there should be little expectation of determining whether the cross-section of (i) or (ii) comes true through measurement with gas discharge in helium, because under the conditions:

$$n_e > 10^{12}\ cm^{-3}\ ,\quad T_e > 3 \times 10^4\ ^\circ K$$

which is needed for the spectral lines of HeII to be observable, the difference in number density between cases (i) and (ii) is already so small that the error in number density due to inaccurate temperature determination is larger than or equal to the difference in number density which is based on the different form of the excitation cross-section. The present results suggest that such an

experimental determination as stated above could be done by more detailed measurements with the TPD plasma; e.g. the best form of the cross-section might have the threshold value between those in case (ii) and (iii), because it is not conceivable that n^{++} at window 4 is larger than those at window 3 and 5 by one order of magnitude. Since n^{++} is obtained as the difference of the two large quantities of n_e and n^+, not a small error must be included in it. However, the values of n^{++} of such an order of magnitude as $10^{11} \sim 10^{12}$ cm^{-3} cannot be deduced from the result[4] given by Drawin; n^{++} is estimated to be only 9.8×10^2 cm^{-3} for $n_e = 10^{14}$ cm^{-3} and $T_e = 2 \times 10^4$ °K.

With the CR (collisional-radiative) model[7] the rate equation relating to the particle densities n^{++}, n^+ and n_e is given by

$$\frac{dn^{++}}{dt} = -\frac{dn^{+}}{dt} = -(\alpha n^{++} - S n^{+}) n_e \ , \qquad (9)$$

where α is the collisional radiative recombination coefficient and S the collisional radiative ionization coefficient; they are functions of n_e and T_e. From eqs.(9) and (6) the time constant as to the change in ion density is found to be $[(\alpha + 2S)(n_o^+ + n_o^{++})]^{-1}$. Here n_o^+ and n_o^{++} are the initial values of n^+ and n^{++}, respectively, and α and S are assumed to be constant; the observed values of n_e and T_e do not remarkably change as far as window 3 from the anode. The followings are estimated from the values given by Bates[7] et al.. For $n_e = 1.28 \times 10^{14}$ cm^{-3} both S and α are 8×10^{-13} cm^3

sec^{-1} at $T_e = 7 \times 10^4$ °K. Since with increasing temperature S increases and α decreases, $\alpha + 2S$ has a minimum value approximately at that temperature, and for lower temperatures it takes values of 2.4×10^{-12} and 4×10^{-11} cm^{-3} sec^{-1} at $T_e = 3 \times 10^4$ and 1×10^4 °K, respectively. For the range of T_e and n_e in question nearly the same results are obtained also with another theory[8] in which the effect of optical thickness for Lyman series and continuum is taken into account. It is therefore possible that doubly ionized ions He^{++} which come out through the anode hole into the "plasma region" and may be produced in the plasma region if T_e is high enough for an atom to be ionized is not yet in a completely steady state at window 4 which is located at a distance of about 80 cm from the anode; the time for an ion to pass through the plasma column can be comparable with or smaller than the time constant estimated from the above, if the ion velocity along the column is assumed to be of the order of 10^5 cm sec^{-1}.

The calculation[9] of population densities of excited levels of hydrogen-like ions in a plasma which is in a quasi-steady state shows that the number density n_i in level i is described in the form

$$\frac{n_i}{(n_i)_{SAHA}} = r_0(i) + r_1(i) \frac{n_1}{(n_1)_{SAHA}} , \qquad (10)$$

where $r_o(i)$ and $r_1(i)$ are the coefficients which are tabulated with n_e and T_e as parameters. Since eq.(10) is obtained from the equation with $i \neq 1$ of eq.(4) under the

conditions

$$\frac{dn_i}{dt} = 0$$

and n_1 is treated as a parameter, it is not possible to determine n_i uniquely from eqs.(10) and (6) only, unless eq.(9) is not solved. Instead of solving it, let the densities at window 4 in case (ii)

$$n_e = 1.83 \times 10^{14} \quad cm^{-3}$$
$$n^+ = 1.77 \times 10^{14} \quad cm^{-3}$$
$$n^{++} = 3.05 \times 10^{12} \quad cm^{-3}$$

be compared with the theoretical ones[9]; by extrapolation with respect to T_e, $r_o(4)$ and $r_1(4)$ are found to be 1.4×10^{-1} and 6×10^{-5}, respectively, for $n_e = 1.28 \times 10^{14}$ cm^{-3}. Equation (10) is rewritten as

$$n_4 = r_o(4)\, n_e n^{++} A(4) + r_1(4) n_1 \exp\left[\frac{E_1}{kT_e}\left(\frac{1}{4^2} - 1\right)\right], \quad (10')$$

where E_1 is the ionization energy of He^+ from its ground level (= 54.4 eV) and A(i) is given by

$$A(i) = \frac{i^2 h^3}{(2\pi m k T_e)^{3/2}} \exp\left(\frac{E_1}{i^2 k T_e}\right) = \frac{4.14 \times 10^{-16}}{[T_e(^\circ K)]^{3/2}} \exp\left(\frac{E_1}{i^2 k T_e}\right).$$

With $r_o(4)$ and $r_1(4)$ estimated above and a reasonable assumption $n_1 \simeq n^+$ eq.(10') gives

$$n_4 = 1.6 \times 10^6 \quad cm^{-3},$$

which is in agreement in order of magnitude with the observed value of n_4 of 2.5×10^6 cm^{-3}. The second term of eq.(10') is only 10^{-21} times as large as the first one; the contribution from n_1 is negligible and the order of magnitude of n^{++} is reasonable. This agreement is rather a natural result, because eq.(7) is essentially the same with eq.(10). Therefore the discrepancy is supposed to be ascribed to the difference of the cross-sections used in the respective eases.

VII. CONCLUSION

When the plasma, which enters the "plasma region" out of the anode hole, comes in contact with a neutral gas, the population densities of the excited levels begin to change with decreasing electron temperature. Recombination of doubly ionized ions He^{++} occurs markedly after their passing through the plasma column downstream from the anode for about as long a time as the relaxation time of collisional radiative recombination. The radiation loss results is decrease in electron temperatrue, which in turn increases the recombination coefficient. Thus the plasma intensely glows white and ion lines with large intensity are radiated through cascading process. Further downstream the recombination of singly ionized ions into neutral atoms becomes dominant; the instantaneous population in a quasi-steady state is presented in a form of a spatial variation along the plasma column. The plasma described in this paper may be considered to be one of light sources suitable for

research of atomic precesses in a plasma on the ground that it has a possibility of presenting data which cannot be obtained in a plasma in a steady state.

ACKNOWLEDGEMENT

The authors wish to express their thanks to Professor T. Takayama for his encouragement to their research with TPD and to Dr. A. Ogata for his help in data processing.

REFERENCES

1. M. P. Freeman: J. Opt. Soc. Am. 50 (1960) 826.
2. O. Gingerich: *Proc. 1st Harvard Smithonian Conf. on Steller Atmospheres* (Cambridge, Mass., 1964) p.17.
3. H. W. Drawin: Ann. Phys. 16 (1965) 195.
4. H. W. Drawin: EUR-CEA-FC-383 (REVISED), 1966.
5. H. R. Griem: *Plasma Spectroscopy* (McGraw-Hill, Inc., 1964)
6. W. L. Wiese, M. W. Smith and B.M. Glennon: *Atomic Transition Probabilities, I, H through Ne, NSRDS-NBS 4,* (National Bureau of Standards, Washington, 1966)
7. D. R. Bates, F. R. S., A. E. Kingston and R. W. P. McWhirter: Proc. Roy. Soc. A 267 (1962) 297.
8. H. W. Drawin: EUR-CEA-FC-510 (1969).
9. R. W. P. McWhirter and A.G. Hearn: Proc. Phys. Soc. 82 (1963) 64.
10. S. Kon, M. Otsuka, M. Yamanaka and H. Yoshinaga: Japan J. appl. Phys. 7 (1968) 433.
11. M. Yokoyama, M. Nakatsuka, C. Yamanaka, Y. Izawa and K. Toyada: Phys. Letters 36A (1971) 317.
12. M. Nakatsuka, M. Yokoyama, Y. Izawa, K. Toyoda and C. Yamanaka: Phys. Letters 37A (1971) 169.

FIGURE CAPTIONS

Fig.1. TPD machine.

Fig.2. (a), (b): Intensity distribution of the recombination continuum observed across the plasma column at window 4. (a): at 2790 Å, (b) at 3420 Å. Here × denotes the observed value. The fitting curve is calculated from only the right half (lower half of the plasma column) of the observed values, and reversed about the axis of symmetry. The ordinate is so normalized that the observed value on the axis of symmetry is unity.

Fig.3. (a), (b): Abel transform of the fitting curve. It is so normalized that the central value is unity. The values of the marked point are used for temperature determination.

Fig.4. $\log_{10}(\varepsilon(\lambda)\cdot\lambda^5/\sigma)$ vs. $1/\lambda$. The abscissa is reduced to energy with $E(eV) = 1.23981 \times 10^4/\lambda(\text{Å})$. The numbers represent the radial distance in mm and the electron temperature in eV.

Fig.5. Radial distribution of the electron temperature and the electron density. It is so normalized that the central value is unity, which is indicated in the figure.

Fig.6. Electron temperatures and electron densities n_e^* on the axis of the plasma column. The observed values of several times are shown. ⊙, △, ⊡, ◇, ▽ : the pressure in the "plasma region" is adjusted in such

a way that the observed intensity of HeII 4686 Å shows maximum at window 4. +, ×: the same is done at window 3.

Fig.7. Population densities of the excited levels on the axis of the plasma column. △ : He 3^3D, ⊡ : He 4^1D, ⊙, ◎ : He^+ n = 4.

Fig.8. Population densities divided by the statistical weights vs. the excitation energy. ×: at window 2, △ : at 3, ⊙ : at 4, ⊡ : at 5.

Table 1.

k lower level	j upper level	E_{jk} (eV)	f_{kj}	A_{jk} (s^{-1})	Window 3: $ne^*=2.68\times10^{14}\ cm^{-3}$, $kTe=3.17eV$ C_{kj}	C^*_{kj} (cm^3s^{-1})	C^+_{kj}	F_{jk}	F^*_{jk} (cm^3s^{-1})	F^+_{jk}	n_j (cm^{-3})
1	4	51.01	2.899^{-2}	2.0448^{8}	2.61^{-18}	5.01^{-17}	1.43^{-16}	1.59^{-12}	3.04^{-11}	8.70^{-11}	(2.68^{14})
2	4	10.2	1.193^{-1}	1.34704^{8}	1.44^{-10}	5.15^{-10}	1.15^{-9}	8.97^{-10}	3.22^{-9}	7.16^{-9}	(2.1^{5})
3	4	2.64	8.421^{-1}	1.43776^{8}	1.73^{-7}	2.26^{-7}	3.40^{-7}	2.24^{-7}	2.93^{-7}	4.39^{-7}	(2.1^{5})
	4										2.1^{5}
4	5	1.23	1.038^{0}	4.3184^{7}	1.27^{-6}	1.34^{-6}	1.40^{-6}	1.20^{-6}	1.27^{-6}	1.32^{-6}	3.8^{5}
4	6	1.89	1.793^{-1}	1.23376^{7}	8.34^{-8}	9.99^{-8}	1.28^{-7}	6.73^{-8}	8.06^{-8}	1.03^{-7}	5.6^{5}
4	7	2.29	6.549^{-2}	4.8656^{6}	1.93^{-8}	2.48^{-8}	3.48^{-8}	1.30^{-8}	1.65^{-8}	2.32^{-8}	9.0^{5}
4	8	2.55	3.23^{-2}	2.2784^{6}	7.16^{-9}	9.31^{-9}	1.39^{-8}	4.00^{-9}	5.20^{-9}	7.75^{-9}	(9.0^{5})
4	9	2.73	1.87^{-2}	1.19344^{6}	3.42^{-9}	4.53^{-9}	7.09^{-9}	1.60^{-9}	2.12^{-9}	3.31^{-9}	9.0^{5}
4	10	2.86	1.196^{-2}	6.776^{5}	1.93^{-9}	2.56^{-9}	4.15^{-9}	7.60^{-10}	1.01^{-9}	1.64^{-9}	9.0^{5}
$C\equiv\sum_{i>4}^{10}C_{4i}$					1.39^{-6}	1.48^{-6}	1.59^{-6}				
$F\equiv\sum_{i<4}F_{4i}$								2.25^{-7}	2.96^{-7}	4.46^{-7}	
$A\equiv\sum_{i<4}A_{4i}$				4.8296^{8}							
$C'\equiv\sum_{i<4}n_iC_{i4}$		(s^{-1})			3.71^{-2}	6.1^{-2}	1.10^{-1}				
$F'\equiv\sum_{i>4}^{10}n_iF_{i4}$		(s^{-1})						5.11^{-1}	5.50^{-1}	5.92^{-1}	
$A'\equiv\sum_{i>4}^{10}n_iA_{i4}$		(s^{-1})		3.14^{13}							
S_4 (cm^3s^{-1})					9.08^{-8}						
α_4 (cm^3s^{-1})					6.4^{-14}						
Q_4 (cm^6s^{-1})					2.5^{-28}						

k lower level	j upper level	Window 4: $ne^*=1.8\times10^{14}\ cm^{-3}$, $kTe=0.88eV$ C_{kj}	C^*_{kj} (cm^3s^{-1})	C^+_{kj}	F_{jk}	F^*_{jk} (cm^3s^{-1})	F^+_{jk}	n_j (cm^{-3})
1	4	7.59^{-37}	2.64^{-34}	1.76^{-34}	7.09^{-13}	2.48^{-10}	1.65^{-10}	(1.8^{14})
2	4	1.35^{-14}	1.63^{-13}	5.03^{-13}	3.65^{-10}	4.41^{-9}	1.36^{-8}	(2.5^{6})
3	4	1.01^{-8}	2.82^{-8}	7.38^{-8}	1.14^{-7}	3.18^{-7}	8.34^{-7}	(2.5^{6})
	4							2.5^{6}
4	5	3.06^{-7}	5.10^{-7}	9.69^{-7}	7.92^{-7}	1.32^{-6}	2.51^{-6}	4.0^{6}
4	6	1.04^{-8}	2.20^{-8}	5.15^{-8}	3.96^{-8}	8.39^{-8}	1.96^{-7}	6.0^{6}
4	7	1.59^{-9}	3.85^{-9}	9.85^{-9}	7.03^{-9}	1.70^{-8}	4.34^{-8}	7.8^{6}
4	8	4.67^{-10}	1.24^{-9}	3.25^{-9}	2.11^{-9}	5.60^{-9}	1.47^{-8}	(8.0^{6})
4	9	1.95^{-10}	5.78^{-10}	1.48^{-9}	8.58^{-10}	2.52^{-9}	6.29^{-9}	(8.0^{6})
4	10	9.22^{-11}	2.92^{-10}	7.54^{-10}	3.8^{-10}	1.20^{-9}	3.11^{-9}	(8.0^{6})
$C\equiv\sum_{i>4}^{10}C_{4i}$		3.19^{-7}	5.38^{-7}	1.04^{-6}				
$F\equiv\sum_{i<4}F_{4i}$					1.14^{-7}	3.23^{-7}	8.48^{-7}	
$A\equiv\sum_{i<4}A_{4i}$								
$C'\equiv\sum_{i<4}n_iC_{i4}$		2.53^{-2}	7.05^{-2}	1.85^{-1}				
$F'\equiv\sum_{i>4}^{10}n_iF_{i4}$					3.46^{0}	5.95^{0}	1.17^{1}	
$A'\equiv\sum_{i>4}^{10}n_iA_{i4}$								
S_4 (cm^3s^{-1})		3.80^{-9}						
α_4 (cm^3s^{-1})		1.70^{-13}						
Q_4 (cm^6s^{-1})		8.60^{-28}						

k lower level	j upper level	Window 5: $ne^*=1.06\times10^{14}\ cm^{-3}$, $kT=0.34eV$ C_{kj}	C^*_{kj} (cm^3s^{-1})	C^+_{kj}	F_{jk}	F^*_{jk} (cm^3s^{-1})	F^+_{jk}	n_j (cm^{-3})
1	4	4.78^{-77}	9.27^{-75}	3.05^{-74}	4.28^{-13}	8.07^{-11}	2.66^{-10}	(1.06^{14})
2	4	7.33^{-23}	2.55^{-21}	8.18^{-21}	1.96^{-10}	6.82^{-9}	2.19^{-8}	(2.6^{4})
3	4	3.97^{-11}	3.34^{-10}	1.02^{-9}	5.26^{-8}	4.41^{-7}	1.34^{-6}	(2.6^{4})
	4							2.6^{4}
4	5	1.88^{-8}	6.31^{-8}	1.59^{-7}	4.49^{-7}	1.50^{-6}	4.04^{-6}	4.3^{4}
4	6	1.83^{-10}	9.22^{-10}	2.73^{-9}	2.11^{-8}	1.06^{-7}	3.15^{-7}	5.5^{4}
4	7	1.34^{-11}	8.55^{-11}	2.58^{-10}	3.67^{-9}	2.36^{-8}	6.98^{-8}	7.8^{4}
4	8	2.34^{-12}	1.70^{-11}	5.24^{-11}	1.06^{-9}	7.71^{-9}	2.37^{-8}	(8.0^{4})
4	9	7.32^{-13}	5.63^{-12}	1.67^{-11}	4.44^{-10}	3.42^{-9}	1.01^{-8}	(8.0^{4})
4	10	2.91^{-11}	2.35^{-12}	6.96^{-12}	2.10^{-10}	1.69^{-9}	5.00^{-9}	(8.0^{4})
$C\equiv\sum_{i>4}^{10}C_{4i}$		1.90^{-8}	6.41^{-8}	1.62^{-7}				
$F\equiv\sum_{i<4}F_{4i}$					5.28^{-8}	4.48^{-7}	1.36^{-6}	
$A\equiv\sum_{i<4}A_{4i}$								
$C'\equiv\sum_{i<4}n_iC_{i4}$		1.03^{-6}	8.68^{-6}	2.65^{-5}				
$F'\equiv\sum_{i>4}^{10}n_iF_{i4}$					2.09^{-2}	7.32^{-2}	2.0^{-1}	
$A'\equiv\sum_{i>4}^{10}n_iA_{i4}$								
S_4 (cm^3s^{-1})		3.47^{-12}						
α_4 (cm^3s^{-1})		3.02^{-13}						
Q_4 (cm^6s^{-1})		2.07^{-27}						

Note: read, e.g. $2.899^{-2}=2.899\times10^{-2}$.

Table 2

		n_e	n^+	n^{++}	(cm^{-3})
Window 3	(i)	2.69^{14}	2.67^{14}	5.40^{11}	
	(ii)	2.68^{14}	2.68^{14}	3.20^{11}	
	(iii)	2.68^{14}	2.68^{14}	4.45^{10}	
Window 4	(i)	1.87^{14}	1.73^{14}	7.12^{12}	
	(ii)	1.83^{14}	1.77^{14}	3.05^{12}	
	(iii)	1.74^{14}	1.86^{14}	-6.38^{12}	
Window 5	(i)	1.06^{14}	1.06^{14}	1.32^{11}	
	(ii)	1.06^{14}	1.06^{14}	5.34^{10}	
	(iii)	1.06^{14}	1.06^{14}	-1.39^{11}	

Note: read, e.g. $2.69^{14} = 2.69 \times 10^{14}$.

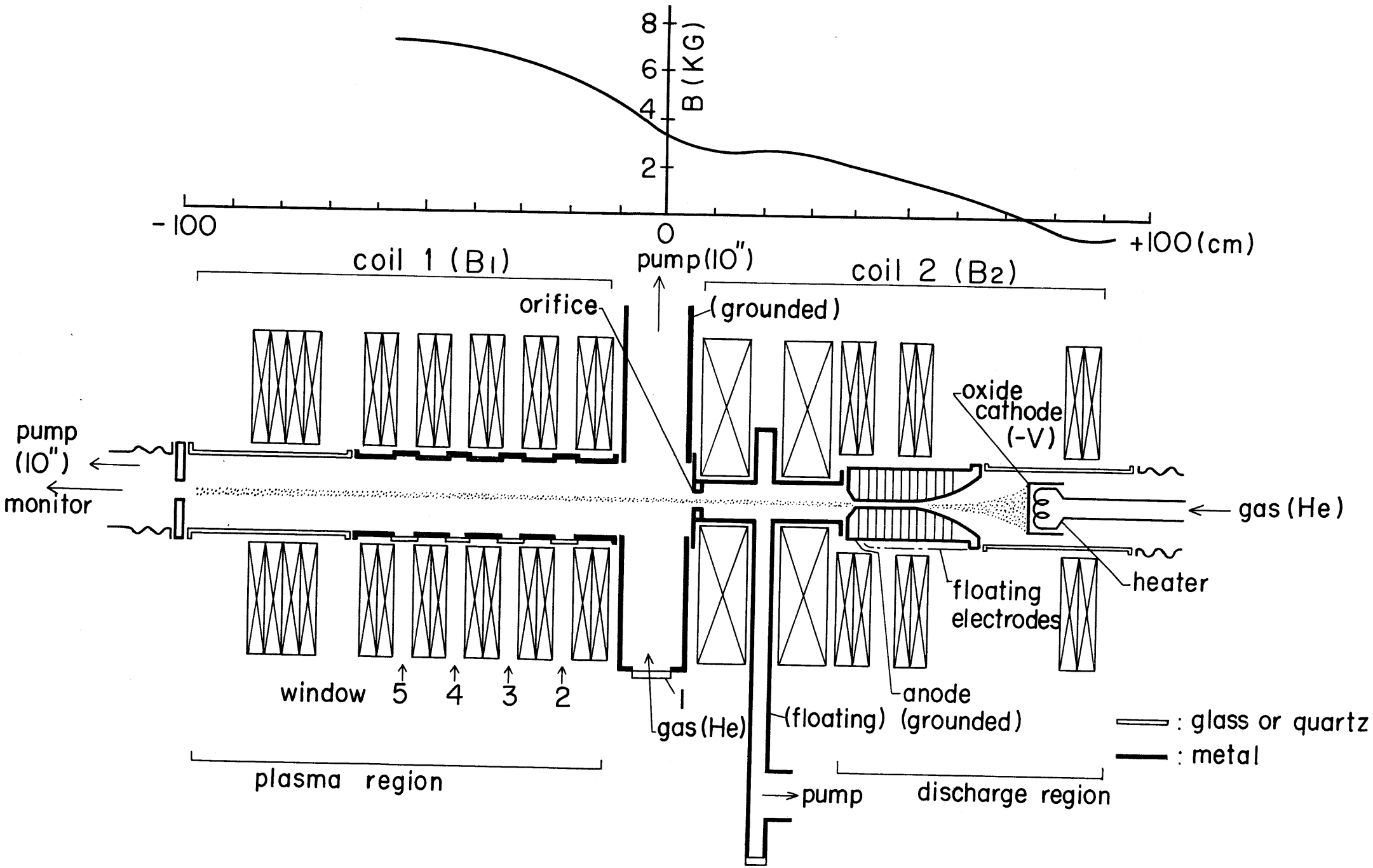
8
6
4
2
B (KG)
-100
0
+100 (cm)
coil 1 (B1)
pump (10")
coil 2 (B2)
orifice
(grounded)
oxide cathode (-V)
pump (10")
monitor
gas (He)
heater
floating electrodes
window 5 4 3 2
1
gas (He)
(floating)
anode (grounded)
: glass or quartz
: metal
plasma region
pump
discharge region

Fig. 1

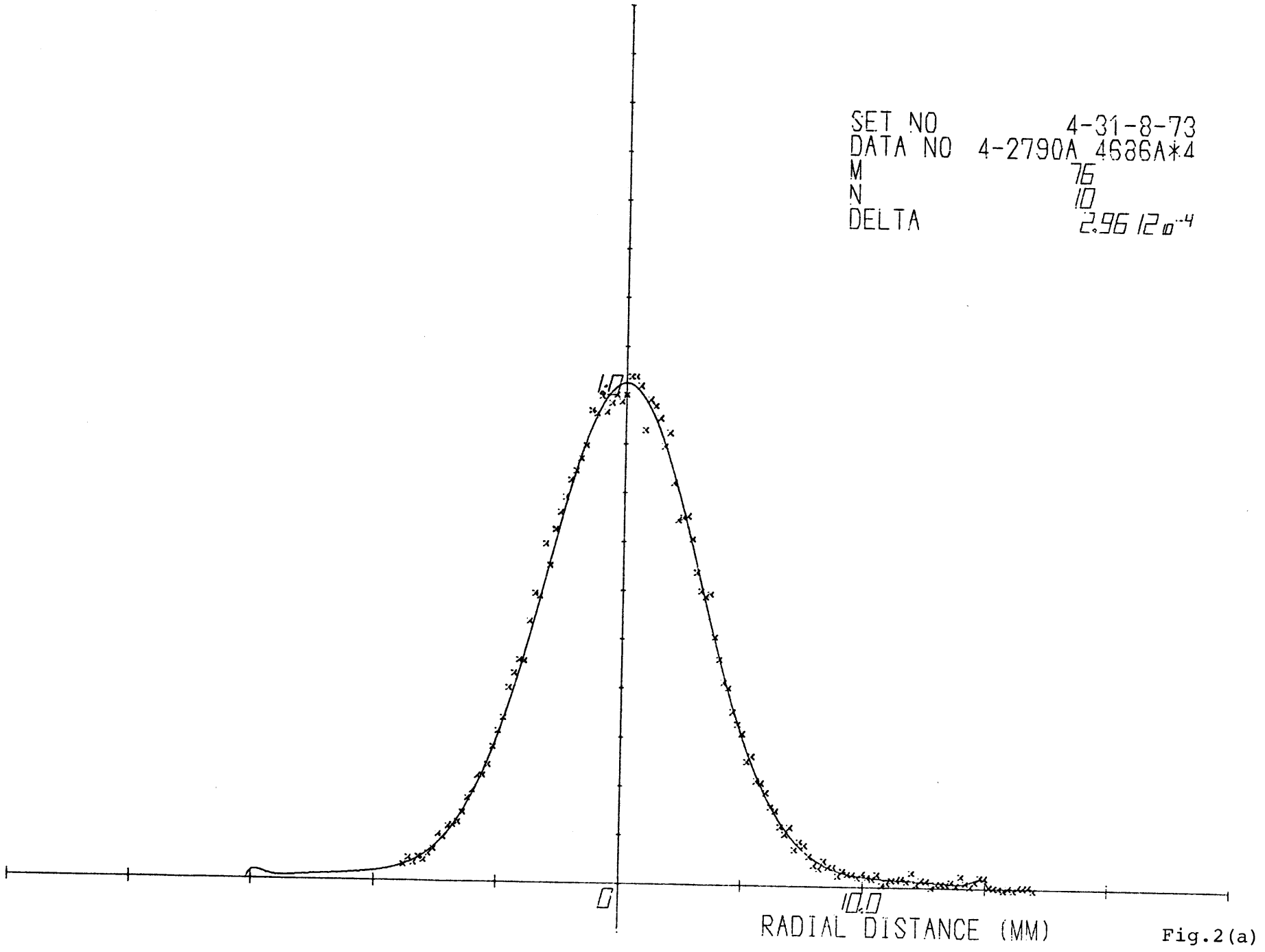
SET NO 4-31-8-73
DATA NO 4-2790A 4686A*4
M 76
N 10
DELTA 2.96 12 10-4
1.0
0
10.0
RADIAL DISTANCE (MM)

Fig.2(a)

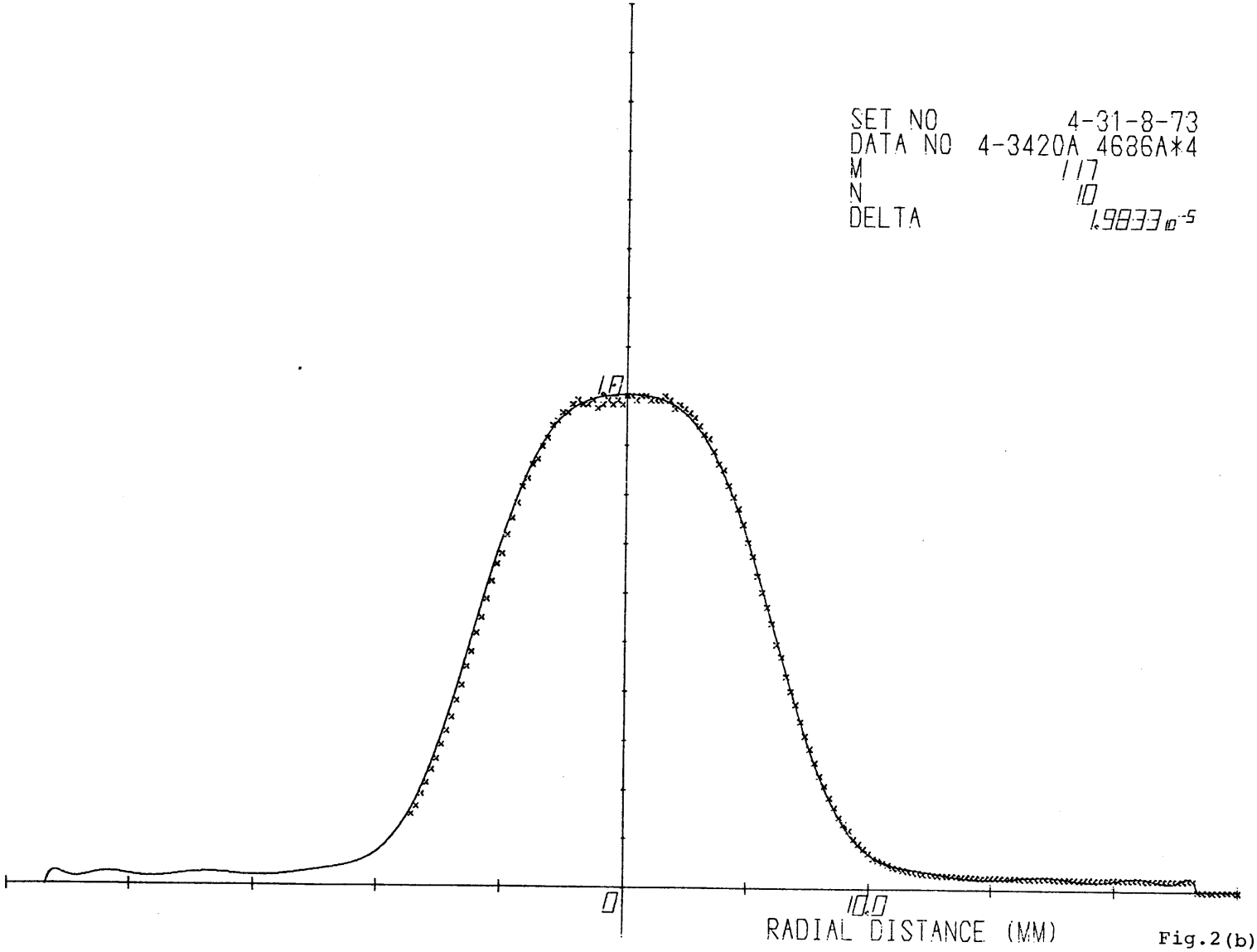
SET NO 4-31-8-73
DATA NO 4-3420A 4686A*4
M 117
N 10
DELTA 1.9833 10-5
1.0
0
10.0
RADIAL DISTANCE (MM)

Fig.2(b)

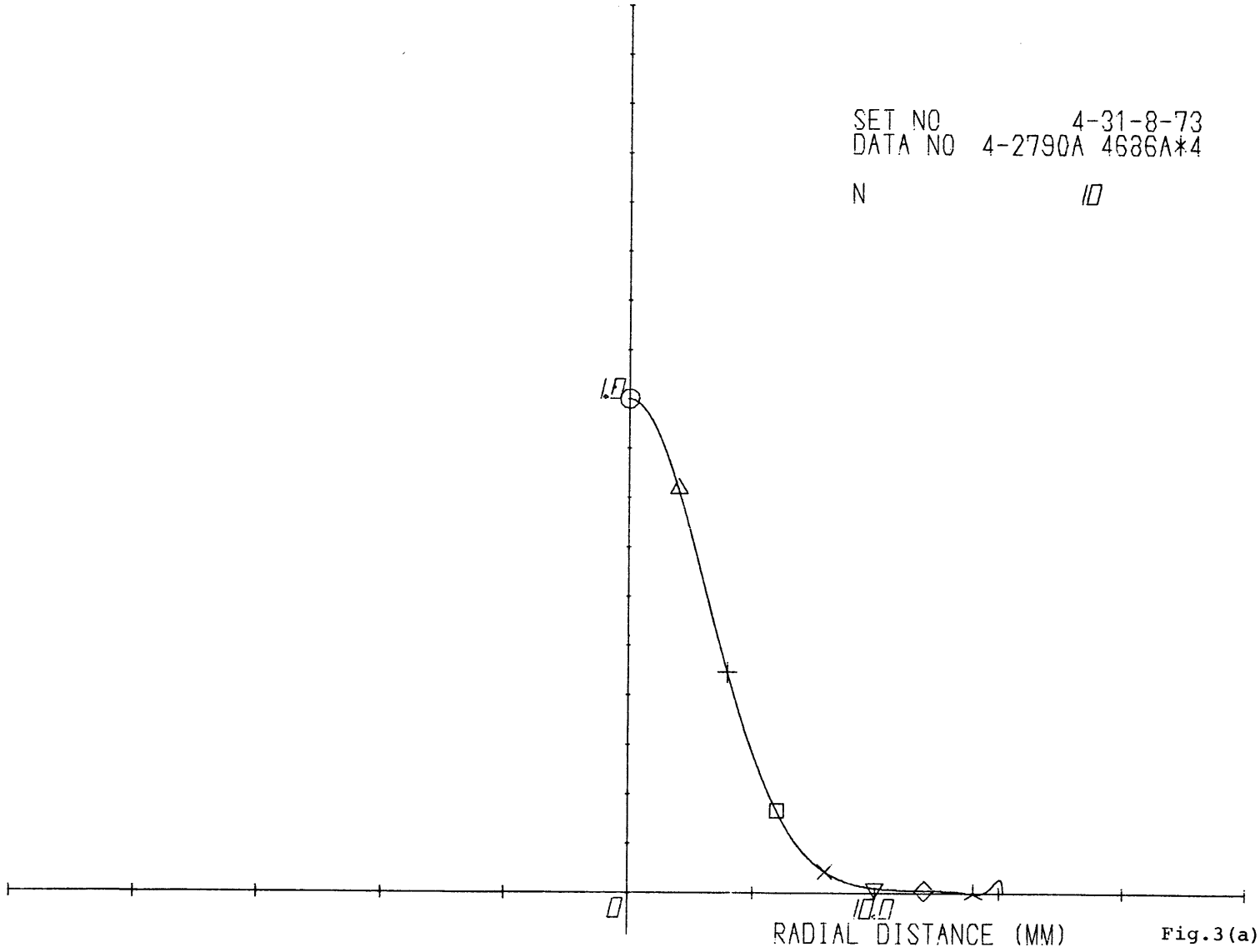
SET NO 4-31-8-73
DATA NO 4-2790A 4686A*4
N 10
1.0
0
10.0
RADIAL DISTANCE (MM)

Fig.3(a)

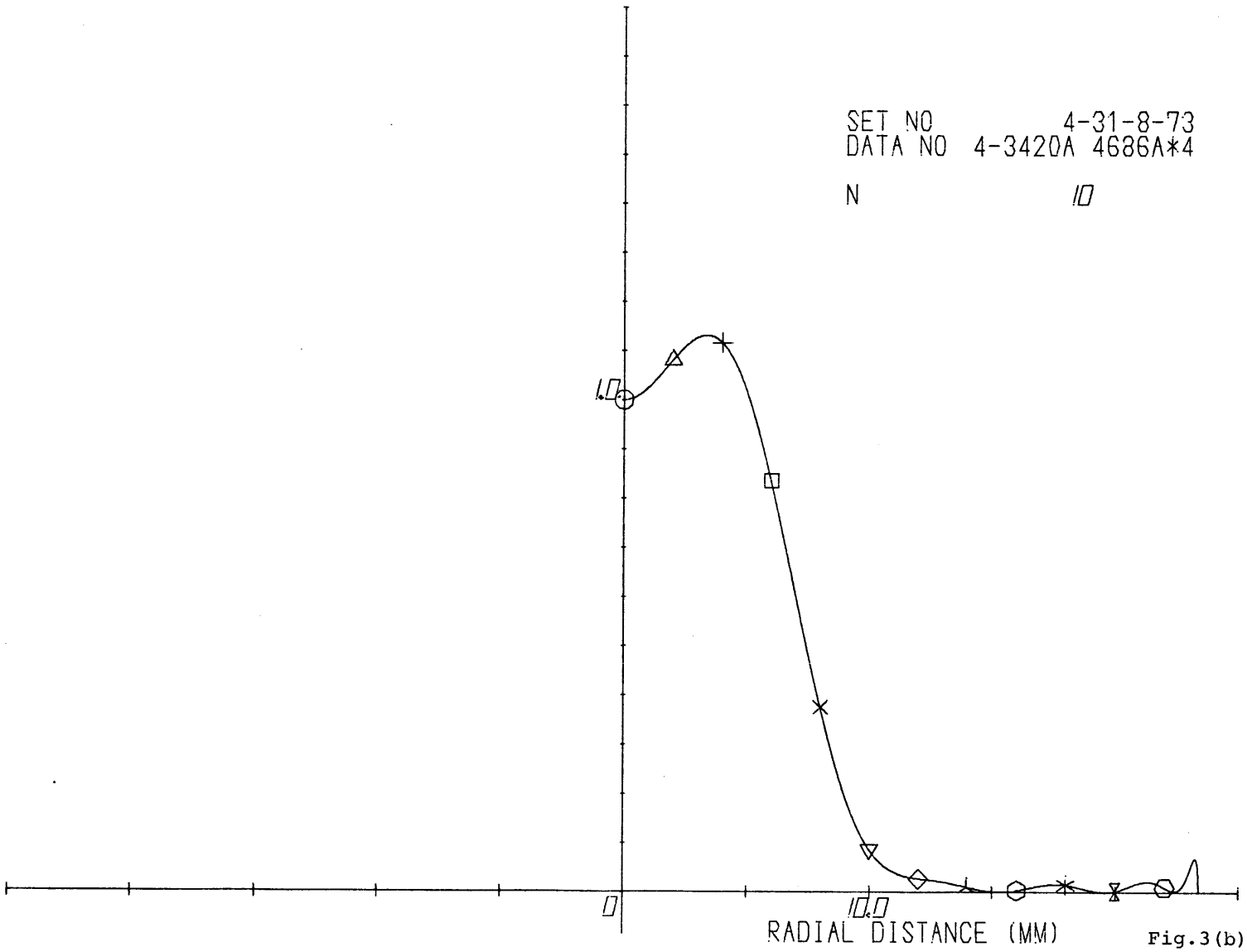
SET NO 4-31-8-73
DATA NO 4-3420A 4686A*4
N 10
1.0
0
10.0
RADIAL DISTANCE (MM)

Fig.3(b)

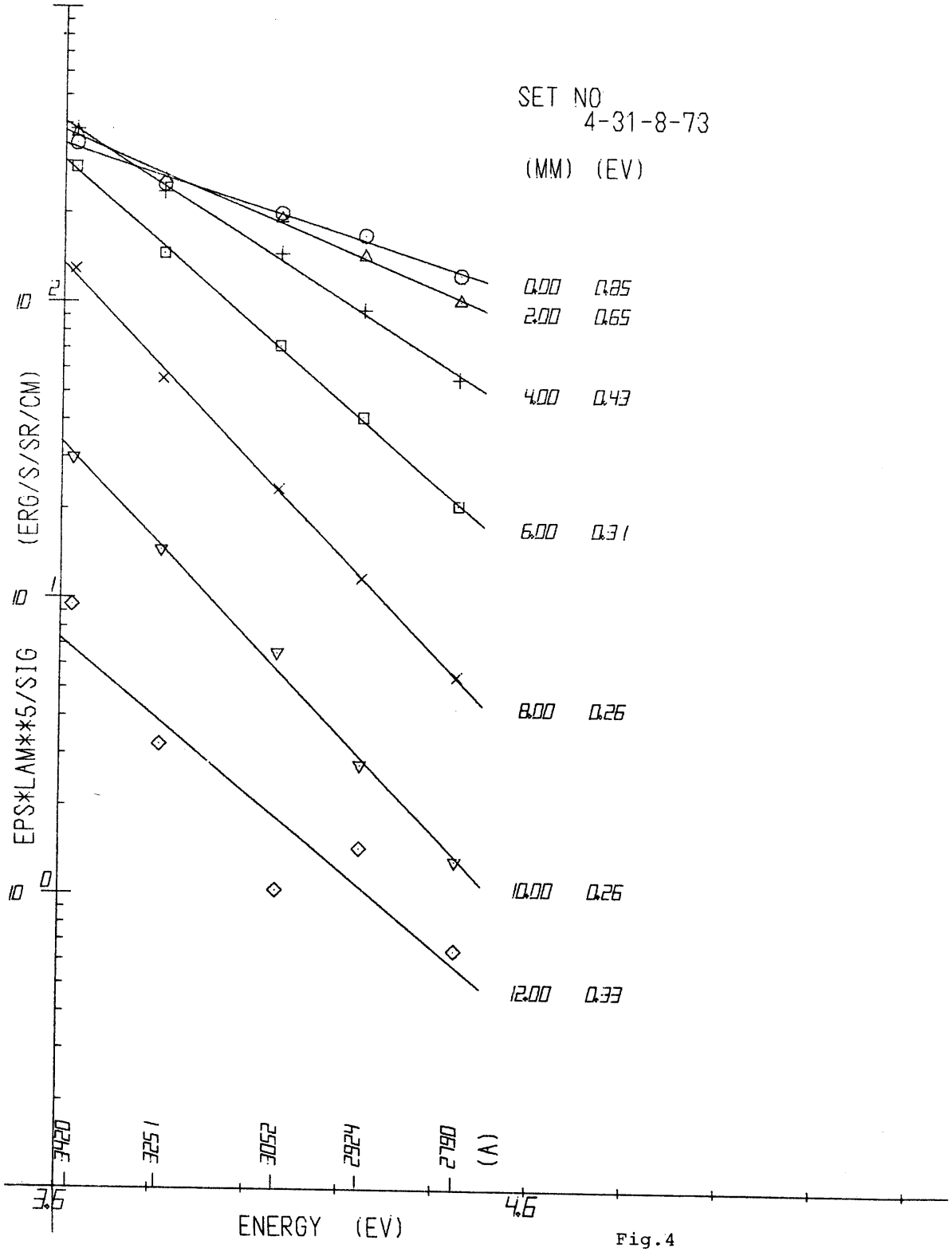
SET NO
4-31-8-73
(MM) (EV)
0.00 0.85
2.00 0.65
4.00 0.43
6.00 0.31
8.00 0.26
10.00 0.26
12.00 0.33
EPS*LAM**5/SIG (ERG/S/SR/CM)
10 2
10 1
10 0
3.6
4.6
ENERGY (EV)
(A)

Fig.4

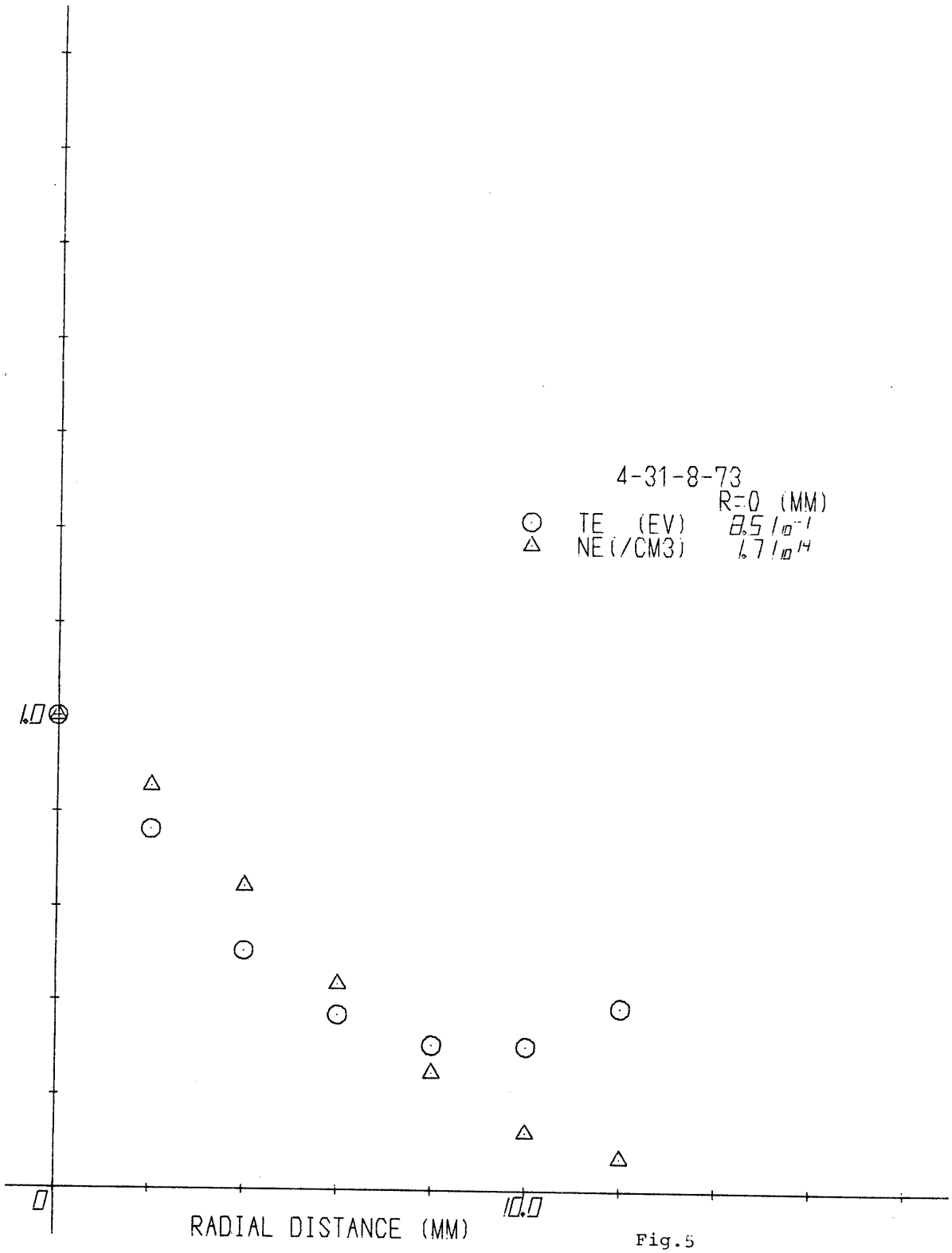
4-31-8-73
R=0 (MM)
TE (EV) 8.5 /10-1
NE(/CM3) 1.7 /10 14
1.0
0
10.0
RADIAL DISTANCE (MM)

Fig.5

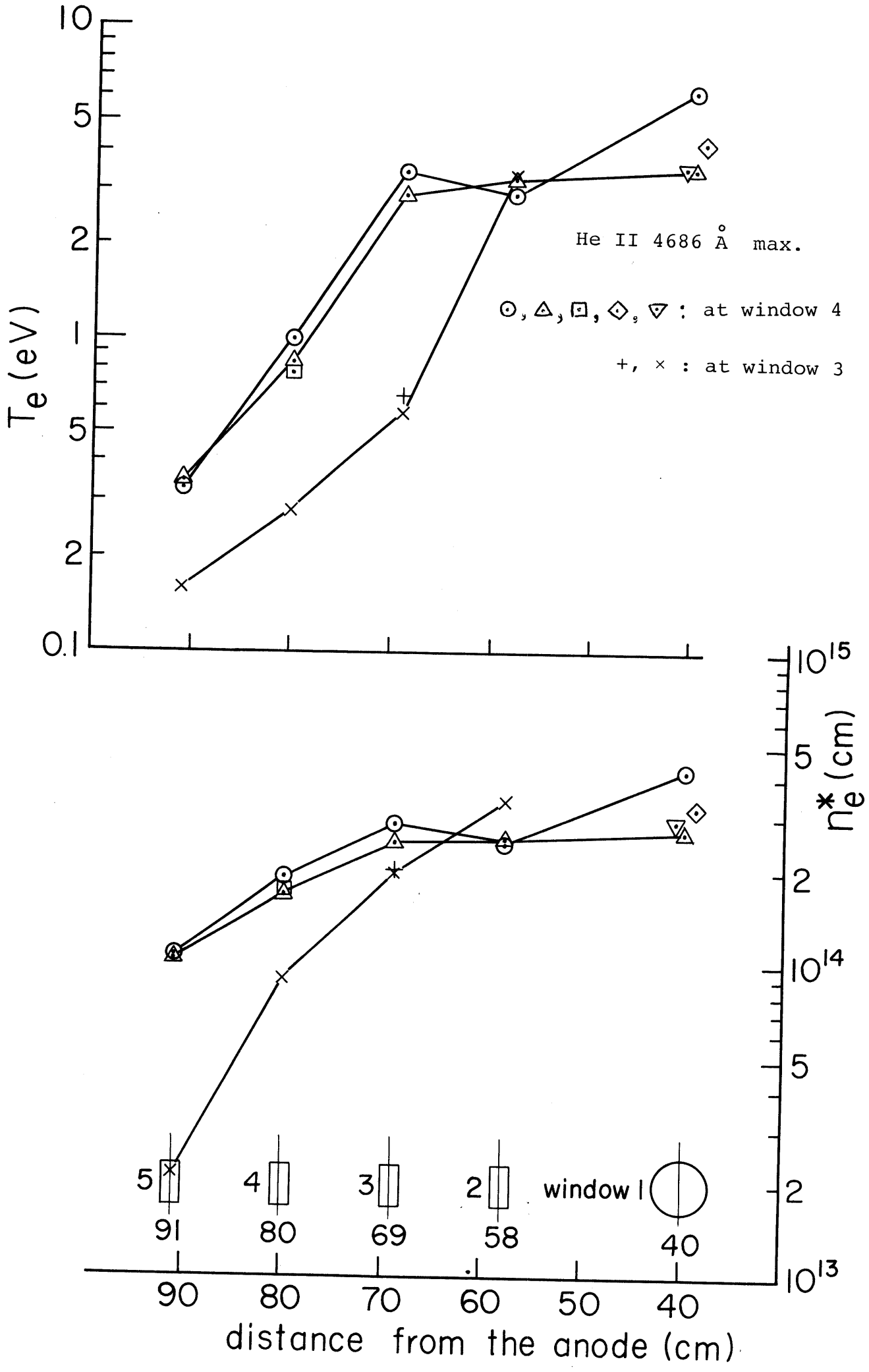
10
5
2
1
5
2
0.1
T_e (eV)
He II 4686 Å max.
⊙, △, ⊡, ◇, ▽ : at window 4
+, × : at window 3
10^{15}
5
2
10^{14}
5
2
10^{13}
n_e^* (cm)
5
4
3
2
window I
91
80
69
58
40
90
80
70
60
50
40
distance from the anode (cm)

Fig. 6

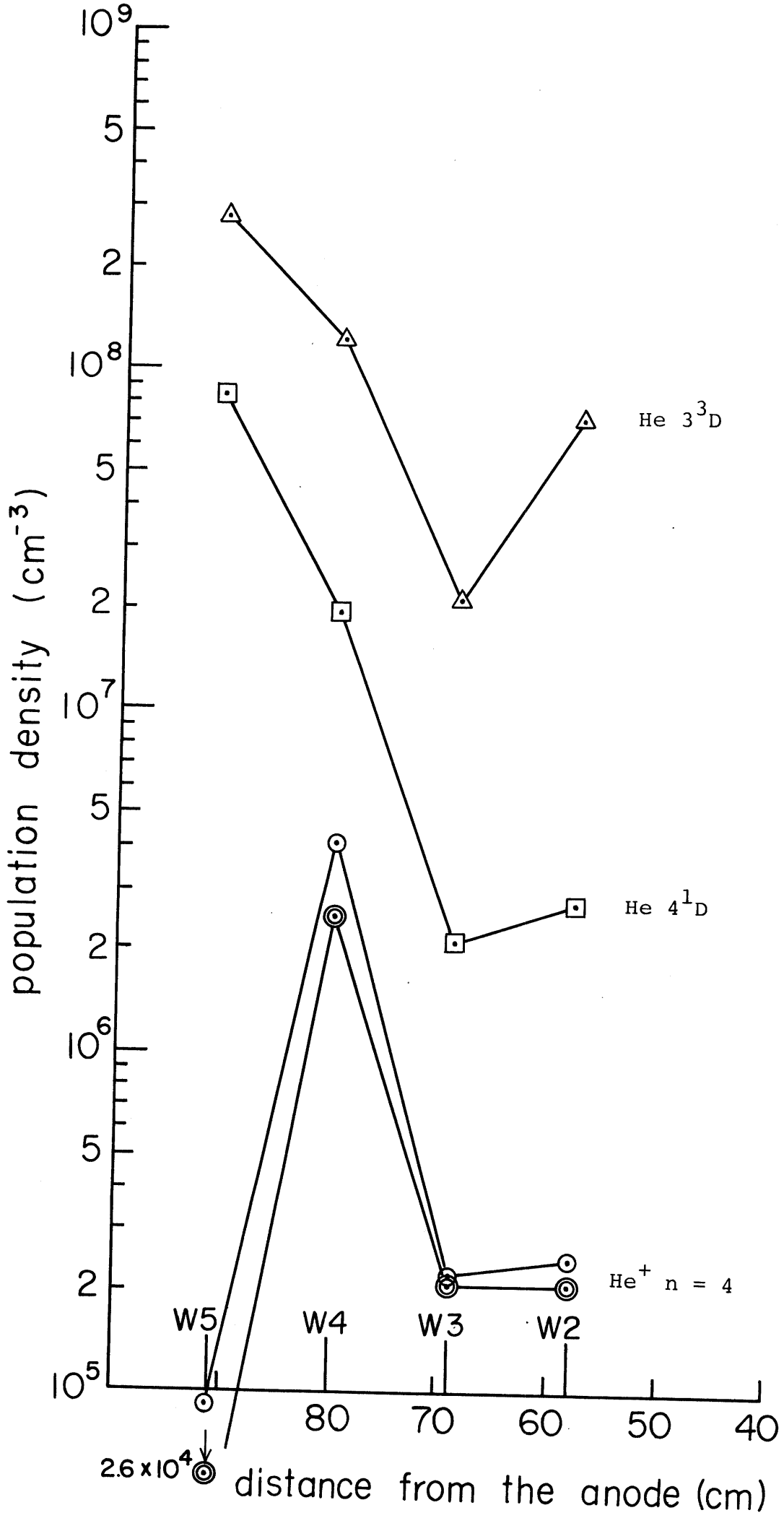
population density (cm^{-3})
10^9
5
2
10^8
5
2
10^7
5
2
10^6
5
2
10^5
He 3^3D
He 4^1D
He$^+$ n = 4
W5
W4
W3
W2
80
70
60
50
40
2.6×10^4
distance from the anode (cm)

Fig. 7

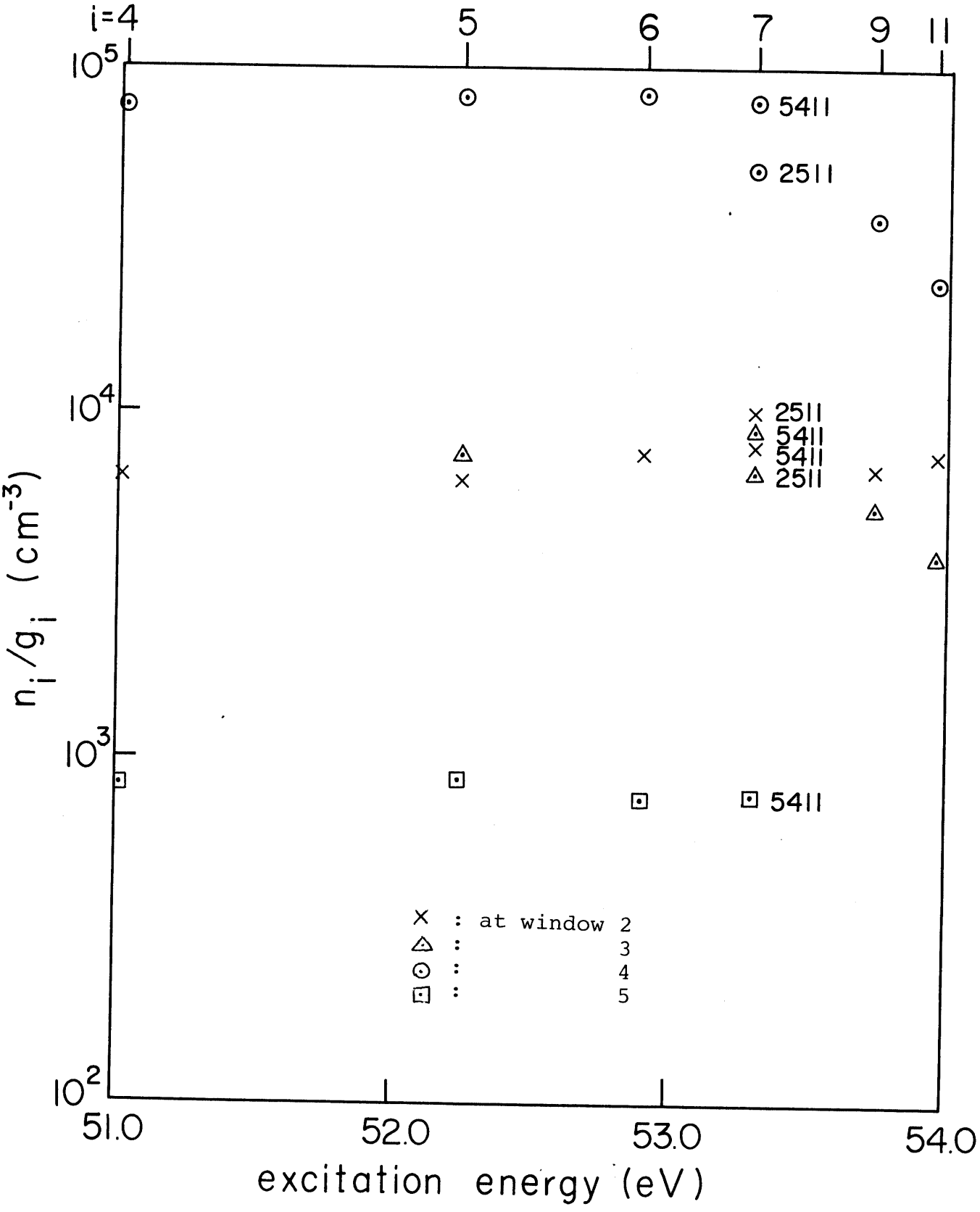
i=4
5
6
7
9
11
10^5
10^4
10^3
10^2
n_i/g_i (cm^{-3})
5411
2511
2511
5411
5411
2511
5411
× : at window 2
△ : 3
⊙ : 4
⊡ : 5
51.0
52.0
53.0
54.0
excitation energy (eV)

Fig. 8